Geomechanics and Engineering, *Vol. 27, No. 3 (2021) 197-211*
https://doi.org/10.12989/gae.2021.27.3.197

Application of artificial intelligence methods for predicting transient response of foundation

Suvendu K. Sasmal[a] and Rabi N. Behera*

Department of Civil Engineering, National Institute of Technology Rourkela, India

(Received July 29, 2020, Revised August 1, 2021, Accepted September 27, 2021)

Abstract. The present work focuses on analysing the displacement of a shallow foundation due to sudden change in state of loading. When a dynamic load hits the foundation, before attaining steady state, the foundation undergoes sudden displacement. This displacement is a function of soil properties viz. modulus of elasticity, Poisson's ratio, loading conditions and the static load already applied on the foundation. A Finite Element based numerical model that considers soil structure interaction is simulated to generate a data set. After verification of model results, the dataset is analysed using five different methods including Levenberg Marquardt Neural Network (LMNN), Bayesian Regularization Neural network (BRNN), Support Vector Machines (SVM), Multivariate Adaptive Regression Splines (MARS) and Multi Gene Genetic Programming (MGGP). A comparative analysis of all the methods has been presented to find out the most effective method. In addition to these, sensitivity analysis is performed to find out the most influencing input parameter. The BRNN method is found to be the most efficient method and the static load on the foundation is the most influencing parameter as revealed from the rigorous statistical analysis. The outcomes will be helpful in quick analysis of shallow strip foundations.

Keywords: artificial intelligence; displacement; sensitivity analysis; shallow strip foundations; soil structure interaction; statistical analysis

1. Introduction

In recent times, with rapid growth in industrialization, the number of structures in and near industrial areas has increased significantly. A stable economic scenario demands stability of these structures throughout the lifetime. The stability and lifetime of any structure are defined, based on the part that actually holds the structure, the foundation. Foundations supporting oscillating machines and foundations very close to machine-dependent industries generally come across dynamic loads in addition to dead load. The behaviour of foundation under dynamic load, apart from the type of load, is controlled by the type of soil beneath the foundation, footing condition and the dead load already applied on the foundation. When a dynamic load strikes the foundation, a set of events takes place near the foundation. Before dynamic loading, the foundation is subjected to only the static load (steady state condition). Upon the striking of the dynamic load, depending on the nature of the load and properties of the underlying soil, the foundation undergoes unexpected shaking. However, before attaining steady state under dynamic load, for a very small duration, just after the hitting of the dynamic load, the foundation undergoes sudden displacement. This response of foundation which remains for a very small duration is termed as the transient response. This transient response is an indication of foundation's capability to resist a sudden, unexpected change of state. While analysing the transient response of footing, it is key to note that dynamic load which act on the foundation can be seismic load, machine-induced load or cyclic load. Cyclic load is the load that repeats its motion after certain time interval. The transient response in case of cyclic load is the response of the foundation when the first load cycle strikes that foundation.

Several literatures are available explaining the cyclic response of foundation. Raymond and Komos (1978) were the pioneers to study the settlement of plane strain footing due to vertical cyclic load. Their study revealed that the settlement is influenced by the properties of soil beneath the footing. Das *et al.* (1995) observed the settlement pattern of square footing under the influence of cyclic loading. The load was applied on the footing in two steps. First a static load is applied followed by the cyclic load. Beam on Nonlinear Winkler foundation model (BNWF), with the help of nonlinear mechanistic spring elements, was used to study the nonlinear response of foundation by Allotey and Naggar (2008), Harden *et al.* (2005).

The aim of Artificial intelligence (AI) techniques is to analyse datasets obtained either from experimental or from numerical analysis. AI methods have been implemented by various researchers, for solving problems related to civil engineering. An Artificial Neural Network (ANN) model was reported by Shahin *et al.* (2002) to

*Corresponding author, Assistant Professor, Ph.D.
E-mail: rnbehera82@gmail.com
[a]Ph.D. Student
E-mail: suvendukumarsasmal@gmail.com

ISSN: 2005-307X (Print), 2092-6219 (Online)

predict the settlement of shallow foundation on cohesionless soil. Das and Basudhar (2006) developed an ANN model for analysis of lateral load capacity of piles on clay. Samui (2008), with the help of support vector machine predicted the settlement of shallow foundation on cohessionless soil. The compaction characteristics and specific gravity of fly ash were predicted by Das and Sabat (2008) using Bayesian regularization neural network (BRNN), differential evolution neural network (DENN) and Levenberg-Marquardt neural network (LMNN). Using different techniques like LMNN, BRNN, DENN and SVM, the swelling pressure of soil was predicted by Das *et al.* (2010). The maximum dry density (MDD) as well as the unconfined compressive strength (UCS) of cement stabilized soil were predicted using different techniques like BRNN, LMNN, DENN and SVM, by Das *et al.* (2011). Erzin and Gul (2013) developed a neural network model to estimate the settlement of pad foundation on cohessionless soil. The amount of settlement of one-way footing was estimated by Erzin and Gul (2014) using Levenberg - Marquardt back propagation learning algorithm**.** Zhang *et al.* (2016) presented LS SVM model for predicting shear strength of soil concrete interface. Xu *et al.* (2017) studied the stability of slope with the help of LS SVM. The 28 days compressive strength of concrete was predicted using multiple linear regression (MLR), ANN and adaptive neuro fuzzy interface system (ANFIS) by Khademi *et al.* (2017). Neural network model for estimating the allowable bearing capacity and elastic settlement of shallow foundation was presented by Omar *et al.* (2018). The Levenberg-Marquardt neural network was used to predict the ultimate bearing capacity of eccentrically inclined loaded shallow strip footing on medium dense and dense sand, by Behera and Patra (2018). Bui *et al.* (2018) developed a hybrid model i.e. combination of modified firefly algorithm and ANN, for analysis of high performance concrete and predicted the compressive and tensile strength. Naderpour *et al.* (2018) predicted compressive strength of environment-friendly concrete using neural network. The elastic modulus of recycled concrete aggregate was calculated by Golafshani and Behnood (2018), using soft computing techniques viz. artificial neural network and support vector regression. Naderpour *et al*. (2018) calculated shear resistance of FRP bars using ANN. Tran *et al.* (2019a) used the concept of ANN for studying square concrete filled steel tubular columns and predicted the axial compression capacity. Rabiei and Choobbasti (2019) designed piled raft system using artificial neural networks. The compressive strength of bentonite and sepiolite plastic concrete was predicted using ANN and SVM by Ghanizadeh *et al.* (2019). Tran *et al.* (2019b) applied soft computing techniques for analysis of circular concrete filled tube. Luat *et al.* (2020a) predicted the settlement of foundation on sandy soil using back propagation algorithm. Luat *et al.* (2020b) developed a hybrid intelligence system based on Bayesian additive regression tree (BART) for analysis of axially loaded circular concrete-filled steel tube (CFST) and calculated the ultimate capacity of CFST. Nguyen *et al.* (2020) predicted axial compressive capacity of CFST using ANN. Hasanipanah (2020) used hybrid artificial neural network for predicting blast induced fly rock. Tran *et al.* (2020) developed an ANN model for the axial compressive capacity prediction of circular CFST columns. Won and Shin (2021) used ANN model for predicting seismic damage, considering soil structure interaction.

Apart from neural network techniques and support vector machines, the output can be expressed in terms of input parameters using techniques like Multivariate Adaptive Regression Splines (MARS) and Genetic Programming (GP). Predictive models for estimating lateral load carrying capacity of piles in clay was reported by Muduli *et al*. (2015) using MARS and GP which were compared with ANN and SVM models. Multi Gene Genetic Programming (MGGP) was used for reliability analysis of liquefaction potential by Muduli and Das (2015). A model was reported by Alavi *et al.* (2017) for determination of flow number of Marshall Specimen using MGGP. The capabilities of MGGP for various complex structural engineering problems were reported by Gandomi and Alavi (2012a). Application of MGGP in different problems, viz. geotechnical engineering and earthquake engineering was reported by Gandomi and Alavi (2012b). MGGP model equations were proposed by Garg *et al.* (2014a) to describe relationship between degree of saturation, suction and net stress of soil. MGGP model for estimating pore water pressure of soil was reported by Garg *et al.* (2014b). Kaveh *et al.* (2018) analysed the stability of a slope using MARS. Gao and Chen (2019) predicted service life of tunnel structures using genetic programming. Khorrami and Derakhshani (2019) predicted the ultimate bearing capacity of shallow foundation on granular soil using GP approach. Luat *et al.* (2020c) predicted the settlement of shallow foundation on sandy soil using MARS. Luat *et al.* (2020d) used MARS for modelling the ultimate capacity of rectangular concrete-filled steel tubular (CFST) columns. Nguyen *et al.* (2020) used machine learning approach for studying compressive strength of green fly ash based geopolymer concrete.

The review of available literature suggests scarcity of works explaining the use of artificial intelligence in the field of cyclic settlement response of foundation supporting a structure. Also, there is lack of empirical equations to estimate the cyclic settlement of footing especially the transient response. In an approach to fill the void, the present study aims at predicting the transient settlement of a shallow strip footing on granular soil with the help of different artificial intelligence techniques. The comparative study presented in the work will be helpful in selecting proper methods while predicting the dynamic response of foundation. Apart from various techniques, the study also discusses significance of input parameters with the help of sensitivity analysis.

2. Finite element analysis

The dataset demonstrating the transient response is obtained with the help of numerical model based on Finite

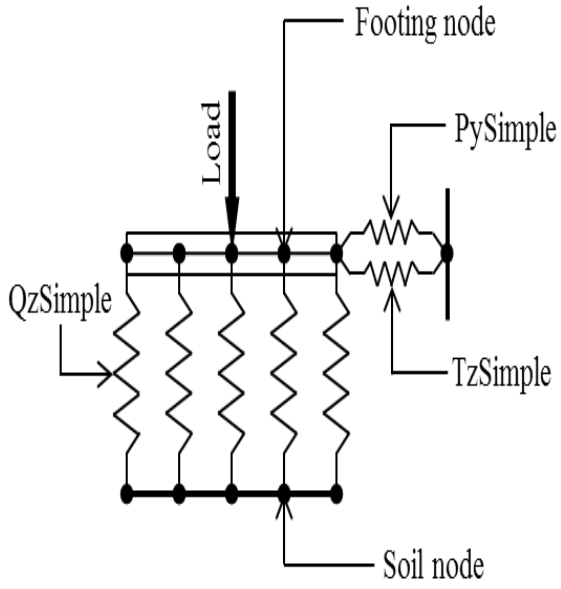

Fig. 1 Components of the BNWF model

Element Analysis. The model is created and analyzed using computer programming tool i.e., Open System for Earthquake Engineering Simulation (OpenSEES).

2.1 Material properties

Beam on Nonlinear Winkler Foundation (BNWF) model is used for numerical modeling of a shallow strip footing. The model is created for a footing resting on granular soil of different relative densities (D_r = 35% (loose), 51% (medium dense), 69% (dense)). The values of soil parameters, viz. angle of internal friction (ϕ) and unit weight of soil (γ) are chosen from existing literature. For loose sand condition, these values are taken from experimental results reported by Sahu *et al*. (2016). For medium dense sand and dense sand conditions, the values reported by experimental study of Patra *et al*. (2012) are used. The ϕ and γ values are 34^0 and 13.34 kN/m^3 respectively for loose sand condition. The ϕ values for medium dense and dense sand are 37.5^0 and 40.8^0 respectively. The γ value for medium dense sand is taken as 13.97 kN/m^3 and its value for dense sand is 14.36 kN/m^3. The values of Poisson's ratio and modulus of elasticity are calculated from EPRI (1990) considering the relative density range provided by Das (2016). The values of Poisson's ratio (v) for loose sand, medium dense sand and dense sand conditions are 0.3, 0.32 and 0.35 respectively. The values of modulus of elasticity (E) for loose sand, medium dense sand and dense sand condition are 20 MPa, 36 MPa and 55 MPa respectively.

2.2 Footing and nonlinear spring elements

The footing is of dimension 0.5 m (Length L) x 0.1 m (width B) x 0.03 m (Thickness t), which is constructed by creating footing nodes and joining them using one dimensional (1D) elastic beam column elements. In the present model, the complete footing comprises of 101 footing nodes and 100 footing elements. The influencing parameters controlling the response of BNWF model like end length ratio, spring spacing and stiffness intensity ratio are chosen according to Harden *et al*. (2005). The footing-soil interface is modeled using nonlinear mechanistic springs. The nonlinear springs are zeroLength elements capable of capturing vertical, passive and sliding responses. Both surface footing and embedded footing conditions have been considered. QzSimple, PySimple and TzSimple springs are used to observe the vertical, passive and sliding response respectively. The values of the stiffness of the springs are assigned as per Gazetas (1991). The nonlinear springs are modelled according to Raychowdhury (2008). The schematic diagram of various components of the present BNWF model is shown in Fig. 1. It shall be noted it is only a schematic diagram. The actual number of footing node considered in this study is 101.

Table 1 Statistical values of the parameters

Parameters	Numeric value			
	Minimum	Maximum	Average	Standard deviation
FS	2	3.5	2.75	0.562
D_f/B	0	1	0.5	0.410
$q_{d(max)}/q_u$ (%)	5	13	9.33	3.315
D_r (%)	35	69	51.66	13.953
s_f/s_u (%)	1.824	14.025	5.935	3.179

2.3 Loading pattern

The loading takes place in two different stages; first an allowable static load is applied on the center of the foundation followed by one cycle of rectangular pulse load. The static load intensity is calculated by dividing the ultimate load carrying capacity (q_u) of the foundation by factor of safety (FS). The values of FS considered in this study are i.e., 2, 2.5, 3 and 3.5. The cyclic load intensity ($q_{d(max)}$) is taken as some percentage (5%, 10% and 13%) of ultimate load capacity of the foundation (q_u). After the application of both static and dynamic loads, the resulting amount of settlement (non-dimensional transient settlement) of the foundation for each case is tabulated in Table A. The statistical values (maximum, minimum, average and standard deviation) of all the parameters (inputs and output) are listed in Table 1.

2.4 Validation of the present model

The preliminary results obtained from the present model have already been verified and presented in Sasmal and Behera (2018). Reasonably good agreement was observed between the results from the BNWF model and

the Mohr-Coulomb model. Moreover, it was also found that for same soil conditions the bearing capacity of the foundation obtained from BNWF analysis matched the calculated value of bearing capacity as per Meyerhof (1963).

3. Dataset pre-processing

In the present work, an attempt has been made to analyse the data with the help of different advanced intelligent methods. The dataset obtained after numerical analysis consists of four inputs and one output. The input parameters are Factor of safety (*FS*), defining the static load on the foundation, embedment ratio (D_f/B), intensity of cyclic load ($q_{d(max)}/q_u$ (%)) and relative density of sand (D_r %). The output is the non-dimensional transient settlement (s_f/s_u) % due to combined influence of static load and the first load cycle. The dataset consists of 108 set of inputs and the corresponding output. Out of total 108 data sets, 81 data sets (75%) are considered for training and remaining 27 data sets (25%) are considered for testing. The details of training and testing data sets are mentioned in Table A. For neural network methods, the data set are normalized in the range of [-1, 1] using the Eq. (1). For MARS and SVM the data set are normalized in the range of [0, 1] using Eq. (2). According to Muduli *et al.* (2015), for genetic programming (GP), normalization is not required.

$$X_{n(ANN)} = 2\left(\frac{X_i - X_{\min}}{X_{\max} - X_{\min}}\right) - 1 \tag{1}$$

$$X_{n(MARS,SVM)} = \left(\frac{X_i - X_{\min}}{X_{\max} - X_{\min}}\right) \tag{2}$$

X_{max} = maximum value of parameter X, X_{min} = minimum value of parameter X.

4. Artificial intelligence techniques

The methodologies adapted in the present study for different artificial intelligence techniques are summarized as below.

4.1 Artificial neural network (ANN)

Artificial neural network techniques are based on the working principle of human brain. In this technique some portion of the entire data (training data set) is trained to build an appropriate predictive model and this model is tested on the remaining portion (testing data set). Two well-known training methods have been considered, i.e. Levenberg Marquardt and Bayesian Regularization. The ANNs based on Levenberg Marquardt and Bayesian Regularization are referred herein as LMNN and BRNN respectively. The LMNN method is based on backpropagation neural network (BPNN), where the error function is the mean square error (MSE). The predicted output is a function of weights and biases obtained after the training. In case of BRNN method, one of the key advantages of regularization method is that overfitting is avoided. The neural network model has three layers. The input layer, the hidden layer and the output layer. The accuracy of the model is controlled by the number of neurons present in the hidden layer in terms of overfitting and underfitting. The LMNN and BRNN algorithms are performed using "trainlm" and "trainbr" functions respectively in MATLAB. Hyperbolic tangent sigmoid function (tansig) and linear transfer function (purelin) are used to develop the ANN model.

4.2 Support vector machines (SVM)

Support Vector Machine (SVM) technique is a well-established method used for classification and regression problems. Support vector machine was used for regression problem by Vapnik *et al.* (1997). Support Vector Regression (SVR) is based on principle of structural risk minimization (SRM). It is one of the most effective methods to predict the required output. The SVR technique is based on ε-insensitive loss function, meaning that errors below ε are neglected. In this method, the input is mapped into high dimensional feature space. The linear model (constructed in the feature space), according to Das *et al.* (2011) is given by;

$$f(x;w) = \sum_{j=1}^{m} w_j \times \Phi_j(x) + b \tag{3}$$

where

$\{\Phi_j(x)\}_{j=1}^{m}$ = feature space representation of input query x

m = support vectors

$w = \{w_0, w_1 \ldots, w_m\}$ = SVM weights

b = bias

The regression steps include minimization of

$$\frac{C}{m}\sum_{i=1}^{m} L_e\left[y_i, f(x_i;w)\right] + \frac{1}{2}\|w\|^2 \tag{4}$$

Subjected to

$L_\varepsilon\left[y; f(x;w)\right] = 0$ for $|f(x;w) - y| < \varepsilon$

Otherwise

$L_\varepsilon\left[y; f(x;w)\right] = |f(x;w) - y| - \varepsilon$

where

$\frac{1}{2}\|w\|^2$ = regularization term, C = capacity factor that determines tradeoff between empirical risk and regularization term

Table 2 Parameters considered for the MGGP model

Parameter	Range
Population size	100, 200, 300
Number of generations	100, 200, 300
Tournament size	2
Maximum number of genes (G_{max})	3, 4, 5
Maximum depth of tree (D_{max})	3, 4, 5
Probability of GP tree mutation	0.1
Probability of GP tree crossover	0.85
Probability of GP tree direct copy	0.05
Total number of models	**81**

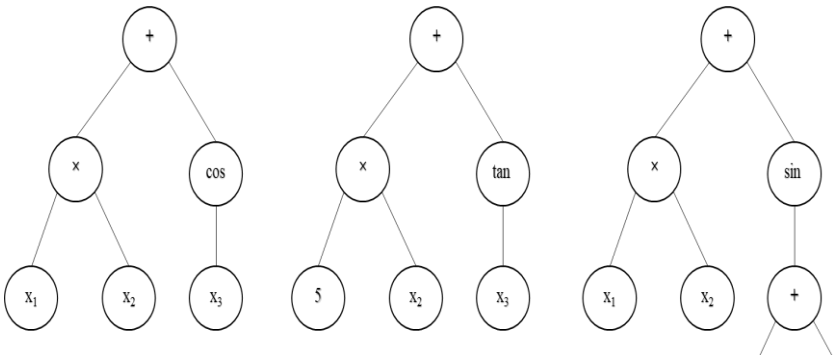

Fig. 2 A typical multi gene model example

The final expression after transferring the optimization problem into quadratic programming problem is given by;

$$f(x) = \sum_{i=1}^{m} (\alpha_i - \alpha_i^*) k(x_i, x) + b \tag{5}$$

Subjected to $0 \le \alpha_i^* \le C, 0 \le \alpha_i \le C$

where

α_i, α_i^* = Lagrange multipliers

The detailed steps can be found in, Samui *et al.* (2008), Smola and Schölkopf (2004).

In the present study, SVR is implemented using the "e1071 package" available in R. The present study considers radial basis function kernel for the SVR model, the expression for which is given by Eq. (6).

$$k(x, x_i) = e^{-\gamma(\|x - x_i\|^2)} \tag{6}$$

The influencing parameters like C and ε are selected on trial and error basis. Default value of γ is taken (γ =1/number of inputs) for the model, which is found to be equal to 0.25. While selecting C and ε, proper care has been taken to avoid over fitting. Over fitting is measured with the help of over fitting ratio calculated with the help of the root mean square error (RMSE). As per Das *et al.* (2010), the over fitting ratio is the ratio of RMSE for testing data to RMSE for training data. As reported by Kurnaz and Kaya (2018), ε has little effect on the performance. The ε parameter is taken in the range of 0.001-0.01@0.001 in this study and emphasis has been given to observe the influence of change in C, which is the regularization parameter. Generally, with increase in C, the R^2 value for training data increases. However, the over fitting ratio also takes very large value for higher C, indicating a poorly generalized model. The optimal value of C is taken as the value beyond which a sudden rise in the over fitting ratio is observed.

4.3 Multivariate adaptive regression splines (MARS)

MARS was developed by Friedman (1991) for the purpose of flexible regression modelling. In this method, the output is predicted in terms of basis functions that conveys information about the inputs and the output. In MARS, the relationship between the inputs and output can be formulated as Eq. (7), given by Samadi *et al.* (2015).

$$Y = f(x) = \beta_0 + \sum_{m=1}^{M} \beta_m h_m(x) \tag{7}$$

where Y = output parameter, x = input variable, β_0 = constant, M = the number of basis functions, $h_m(x)$ is the m^{th} basis function, β_m = corresponding coefficient of $h_m(x)$.

The basis function $h_m(x)$ can be defined as;

$$h_m(x) = \max(0, c - x) \tag{8}$$

or

$$h_m(x) = \max(0, x - c) \tag{9}$$

where c = threshold value for x

In the present study, MARS analysis including training and testing is performed using the "earth" package available in computational platform "R". The process consists of two steps i.e., the forward pass and the pruning pass. After the forward pass a basis matrix is obtained which has a row for every observation as well as a column for every basis function. The role of pruning pass is to obtain the subset that gives the lowest Generalized cross validation (GCV). The GCV is expressed in the form of Eq. (10) given by Zhang and Goh (2016).

$$\text{GCV}= \frac{\frac{1}{N}\sum_{i=1}^{N}[y_i - f(x_i)]^2}{\left[1-\frac{M+d\times(M-1)/2}{N}\right]^2} \quad (10)$$

where;
M = number of Basis functions (BF), d = penalty for each BF, N = number of data, $f(x_i)$ = MARS predicted values.

4.4 Multi gene genetic programming (MGGP)

In the present study, multigene symbolic regression is preformed to predict the output in terms of the input parameters using Multi Gene Genetic Programming which is an evolutionary approach. A compact summary of the MGGP algorithm is presented in this section. Initially, several controlling parameters are defined by the user. Then an initial population is generated with the help of randomly selected functions and terminals. Genetic operations like mutation, crossover and reproduction are applied to form the new population. Generally, the process continues until the one of the termination criteria is met. The termination criterion is either the number of generations or the threshold error. In MGGP, the final outcome is a result of weighted linear combination of several GP trees known as genes. The expression takes the form of Eq. (11) as per Searson (2009).

$$\hat{y} = d_0 + d_1 \times tree\ 1 + ... + d_M \times tree\ M \quad (11)$$

where, d_0 = bias term, $d_1 \ldots . d_M$ = gene weights

An example of the GP tree is presented in Fig. 2. The expression for Fig. 2 will be,

$$d_0 + d_1(x_1x_2 + \cos x_3) + d_2(5x_2 + \tan x_3) + d_3(x_1x_2 + \sin(x_3 + x_4)) \quad (12)$$

The MGGP model is simulated using GPTIPS available in MATLAB platform. The accuracy of MGGP model depends on parameters listed in Table 2. A total number of 81 MGGP models have been run to select the best set of combination, based on parameters mentioned in Table 2. The parameters are selected following Searson (2009), Searson *et al.* (2010). With increase in maximum number of genes (G_{max}) and maximum depth of tree (d_{max}), the model performance generally increases, however the chance of model over fitting increases, making the generalization of the model difficult. For the sake of developing a less complex and more generalized model, the values of G_{max} and d_{max} are taken as 3, 4 and 5.

5. Results and discussions

The results obtained from each of the artificial intelligence methods are discussed sequentially. In this section, first the observed output is compared with the outputs from all the five methods, followed by sensitivity analysis of the input parameters. In neural networks, the selection of number of neurons in the hidden layer is performed by observing the variation of MSE with an increase in number of hidden layer neurons as shown in Fig. 3. It is observed from Fig. 3 that the minimum MSE is observed when the number of neurons in hidden layer is 5. Hence, both the models (LMNN, BRNN) take the form of 4-5-1 architecture. The artificial neural network architecture is shown in Fig. 4.

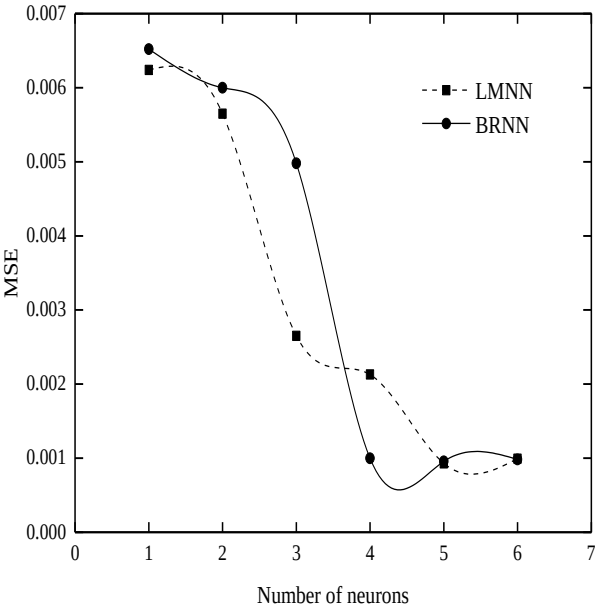

Fig. 3 Performance of neural network with increasing hidden layer neuron

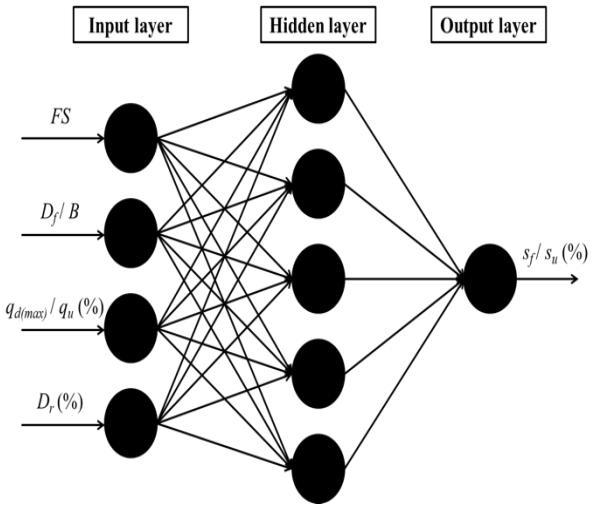

Fig. 4 ANN architecture

Table 3 Values of weights and biases (LMNN)

Hidden layer Neuron	Weights						Bias
	w_{ik}				w_k		
	FS	D_f/B	$q_{d(max)}/q_u$ (%)	D_r(%)	s_f/s_u (%)	b_{hk}	b_0
1	0.1841	3.1723	0.0188	2.4230	-0.2991	2.6233	
2	0.3969	0.7021	0.0250	0.2871	0.6122	0.4800	
3	3.2616	0.5890	-1.4574	-0.5033	-0.0515	-1.9807	1.5653
4	0.7417	1.1325	-0.1307	-2.3884	-0.3018	2.9876	
5	-0.6262	-0.0816	0.1196	-0.1180	2.5131	-1.0201	

Table 4 Values of weights and biases (BRNN)

Hidden layer Neuron	Weight						Bias
	w_{ik}				w_k		
	FS	D_f/B	$q_{d(max)}/q_u$ (%)	D_r(%)	s_f/s_u (%)	b_{hk}	b_0
1	0.2348	-0.0945	-0.0408	-0.8569	0.7242	0.1857	
2	0.4679	-0.0096	-0.1999	-0.1217	-0.5951	-0.0446	
3	0.1348	0.6684	-0.0377	-0.7015	-0.4845	0.9529	0.8335
4	0.9967	0.0494	-0.1693	0.1004	-1.1878	1.2574	
5	-0.1728	0.9461	0.0155	1.2858	0.4244	-0.8178	

The obtained values of weights and biases from the LMNN and BRNN methods are tabulated in Table 3 and Table 4 respectively. Based on the weights and biases, the predicted outputs are obtained and compared with the output from the FEM model. Fig. 5 shows the comparison between the observed and predicted outputs for LMNN and BRNN method indicating the prediction accuracy of both the models. For LMNN method, the values of R^2 for training and testing are found to be 0.9966 and 0.9928 respectively. R^2 values for training and testing are 0.9965 and 0.9929 respectively in the case of the BRNN method. R^2 is calculated using Eq. (13). These numeric values indicate good learning and generalization capabilities of the above mentioned models. The neural network model equation with the help of weights and biases takes a form as shown in Eq. (14) given by Goh *et al.* (2005).

$$R^2 = \frac{E_1 - E_2}{E_1} \tag{13}$$

where;

$$E_1 = \sum_{i=1}^{n} \left(O_i - O_a\right)^2 \text{ and } E_2 = \sum_{i=1}^{n} \left(O_p - O_i\right)^2$$

where; O_i, O_a and O_p are observed, average observed and predicted values of $(s_f/s_u)\%_n$ respectively.

$$(s_f / s_u)\%_n = f_n\left\{b_0 + \sum_{k=1}^{h}\left[w_k f_n\left(b_{hk} + \sum_{i=1}^{m} w_{ik} X_i\right)\right]\right\} \tag{14}$$

where, $(s_f/s_u)\%_n$ = normalized value of non-dimensional transient settlement, f_n = transfer function, h = number of neuron in hidden layer, X_i = normalized value of input, m = number of input variables, w_{ik} = connection weight between i^{th} layer of input and k^{th} neuron of hidden layer, w_k = connection weight between k^{th} neuron of hidden layer and single output neuron, b_{hk} = bias at k^{th} neuron at hidden layer, b_0 = bias at output layer.

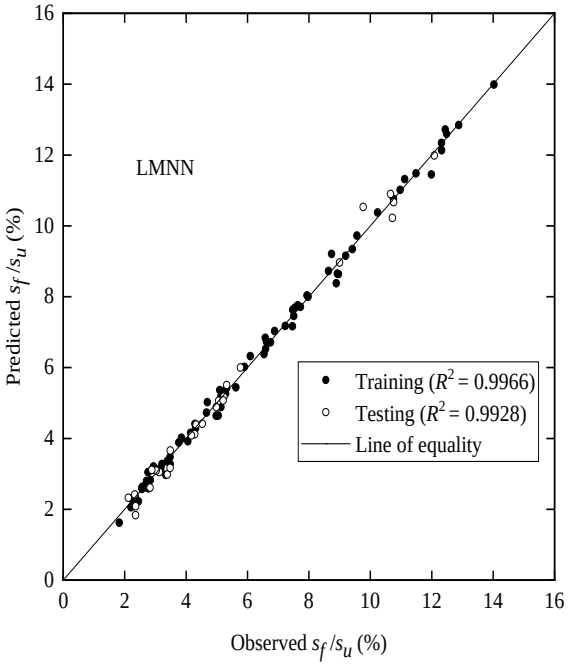

(a)

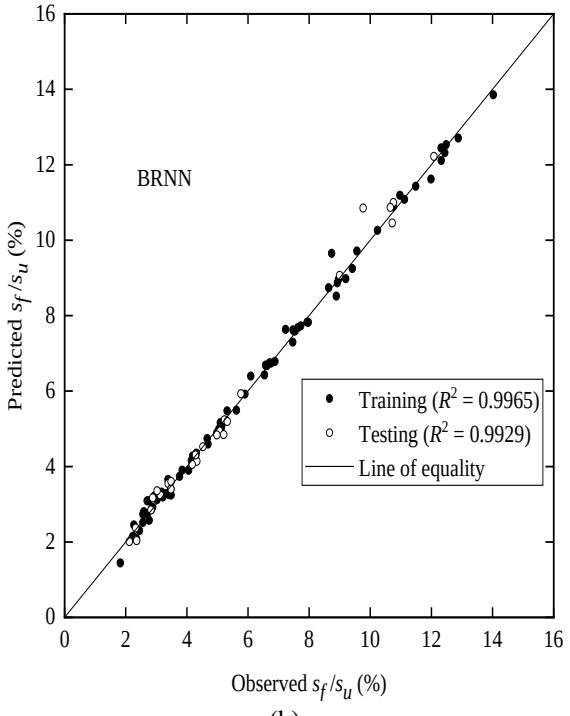

(b)

Fig. 5 Comparison of observed output with the output obtained using (a) LMNN and (b) BRNN

The performance of SVR model is significantly controlled by the selection of parameters. The optimal values of ε and C are found to be 0.01 and 6 respectively. Using the optimum values of parameters, the outputs

Table 5 Basis functions and coefficients obtained from the MARS model

Basis function (BF)	Equation	Coefficient
BF1	max (0, 0.333-x_1)	1.049
BF2	max (0, x_1-0.333)	-0.568
BF3	max (0, x_1-0.667)	0.209
BF4	max(0, 0.5-x_2)	0.093
BF5	max (0, 0.625-x_3)	-0.164
BF6	max (0, x_3-0.625)	0.238
BF7	max (0, 0.471-x_4)	0.126

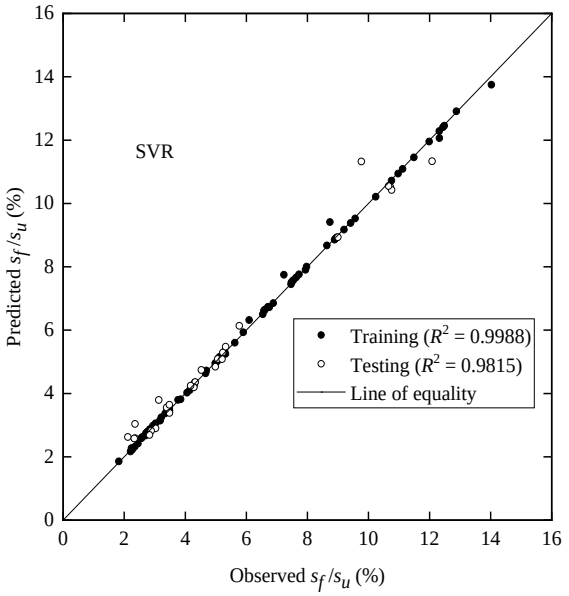

Fig. 6 Comparison of observed output with the output obtained using SVR model

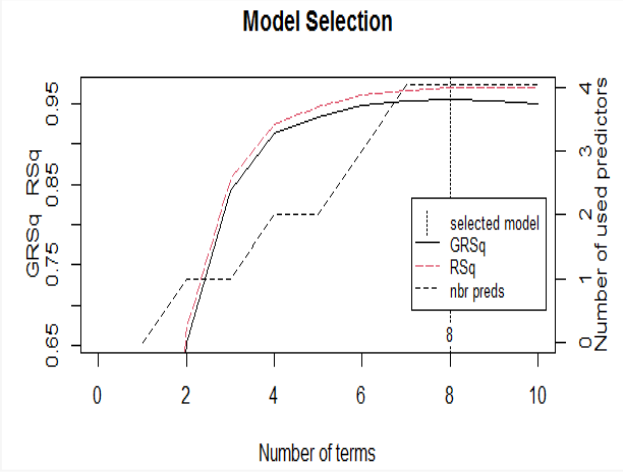

Fig. 7 Selection of number of basis functions for MARS model

obtained from the SVR model are compared with the observed output in Fig. 6 indicating R^2 values of 0.9988 and 0.9815 for training and testing respectively. It is observed from the Fig. 6 that the SVR model is very well trained with a better R^2 value for training than those of

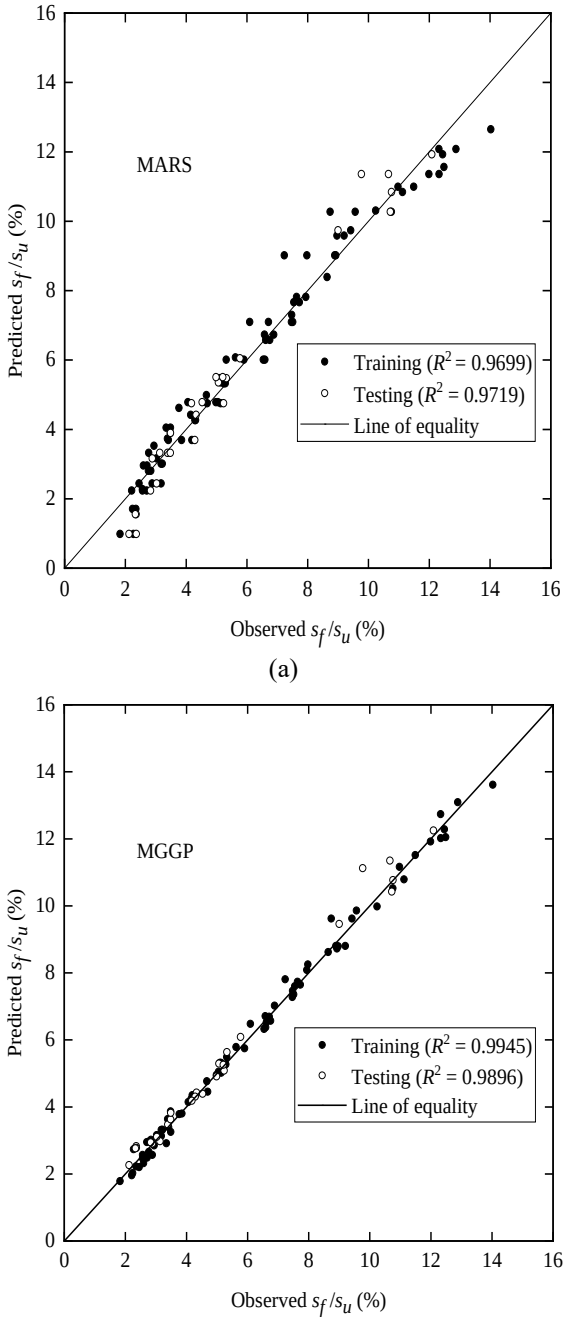

Fig. 8 Comparison of observed output with the output obtained using (a) MARS (b) MGGP

neural networks (LMNN, BRNN). However, the R^2 obtained for testing set is found to be a little less than those obtained by both LMNN and BRNN.

The basis functions obtained from MARS are presented in Table 5. The MARS model is simulated by considering all the default values. The defaults value of degree of interaction is "1". It is well known that with increase in degree of interaction the complexity of the model increases. In this work, the model prediction accuracy is satisfactory even for degree of interaction = 1. The default penalty value is 2. The default nprune is NULL. The best model is selected based on R^2 (RSq)

Table 6 RMSE, MAE and MAPE values calculated for different methods

Method	RMSE training	RMSE testing	MAE training	MAE testing	MAPE training	MAPE testing
LMNN	0.186	0.264	0.139	0.201	0.028	0.049
BRNN	0.189	0.277	0.136	0.189	0.030	0.042
SVR	0.111	0.421	0.054	0.273	0.009	0.064
MARS	0.554	0.631	0.421	0.504	0.088	0.135
MGGP	0.237	0.373	0.186	0.252	0.038	0.055

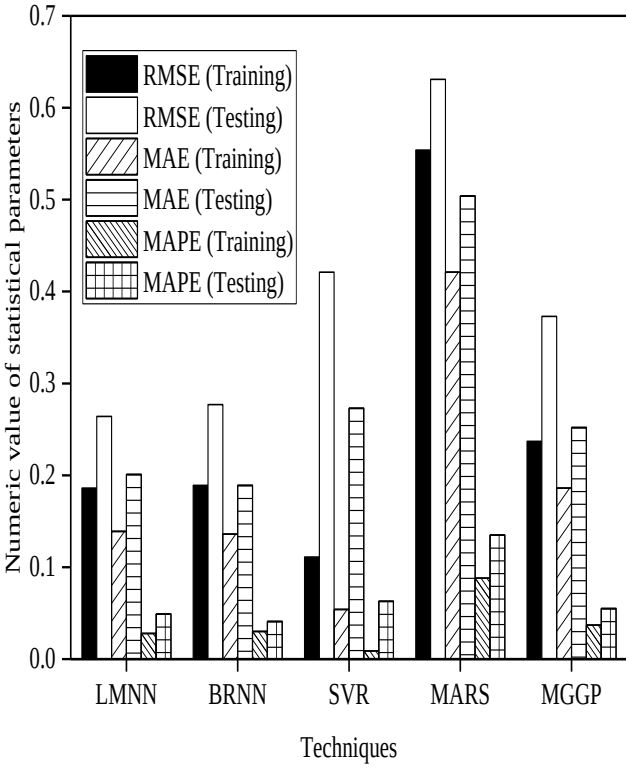

Fig. 9 Comparison of the RMSE, MAE and MAPE obtained for different methods

and Generalized R^2 (GRSq). The GRSq standardizes raw value of GCV in a similar way the R^2 standardizes residual sum of squares. The number of basis function is equal to 7. The total number of terms in the MARS equation will be 8 (including intercept) as shown in Fig. 7. For the MARS model, the value of intercept found to be 0.343. Using the values of the coefficients listed in Table 5 and the intercept, the expression for calculating $(s_f/s_u)\%_n$ is given by Eq.(15). The predicted outputs based on the intercept and basis functions are compared with the observed values as shown in Fig. 8(a). R^2 values for training and testing are 0.9699 and 0.9719 respectively. It is found that the MARS model has reasonably good ability to predict output, outside training data set, as R^2 for testing data is more than that of training data.

$$(s_f/s_u)\%_n = 0.343 + 1.049\times BF1 - 0.568\times BF2 + 0.209\times BF3 + 0.093\times BF4 - 0.164\times BF5 + 0.238\times BF6 + 0.126\times BF7 \quad (15)$$

After the single independent run of 81 model conditions, the optimum MGGP model is taken as the one which delivers the best R^2 value for the testing data set. For optimum MGGP model, the R^2 for training data is 0.9945 and for testing data is 0.9896. The model equation developed using the coefficients, is given by Eq. (16). The outputs from the best MGGP model are compared with the observed output along with R^2 of training and testing data in Fig. 8(b).

$$s_f/s_u(\%) = 0.5929\times x_3 + 0.0006\times\Big(\big(\cos(\exp(x_1\times x_2))\big) - \big((x_3 - \cos(x_4))\times\big(\cos(x_4) - (x_3^2)\big)\big)\Big) + 0.7212\times\big(\big(\cos(\exp(x_2\times x_4))\big) - \big(\cos(x_1 - \cos(x_4))\big)\big) + 346.5992\times\big(\tanh(\tanh(\cos(\tanh(x_1))))\big) + 0.2037\times\big(\big(\cos(x_2 + (x_1\times x_3))\big) + \big(\cos(x_1)\big) - \big(\sin(x_4)\big)\big) - 0.1737\times\big(\big(\cos(x_2\times x_4)\big) + \big(\big(\tanh(x_4)\big)\times\big(\cos(x_2) + (x_1\times x_3)\big)\big)\big) - 156.2866 \quad (16)$$

Although all the considered methods have very good prediction ability, a comparison is established among the methods to find out the best method. In addition to R^2, the Root mean square error (RMSE), Mean absolute error (MAE) and the Mean absolute percentage error (MAPE) values for training data sets and testing data sets are obtained for each method. The RMSE, MAE and MAPE are calculated using Eqs. (17), (18) and (19) respectively. The calculated values are listed in Table 6. A graphical comparison is presented in the form of Fig. 9. The best technique is selected by considering these values for testing dataset. Similar approach was followed in existing literature such as Das *et al.* (2011), Shahin (2015) and Muduli and Das (2015).

$$RMSE = \sqrt{\frac{1}{n}\sum_{i=1}^{n}(O_i - P_i)^2} \quad (17)$$

$$MAE = \frac{1}{n}\sum_{i=1}^{n}|O_i - P_i| \quad (18)$$

$$MAPE = \frac{1}{n}\sum_{i=1}^{n}\left|\frac{O_i - P_i}{O_i}\right|\times 100 \quad (19)$$

where n = number of data points, $O_i = i^{\text{th}}$ observed output, $P_i = i^{\text{th}}$ predicted output.

For training set, the lowest values of RMSE, MAE and MAPE are obtained when the training algorithm is support vector regression (SVR). For testing set, lowest RMSE is obtained for LMNN model whereas lowest MAE and MAPE values correspond to the BRNN model. Also as discussed earlier, the highest value of R^2 for testing data is obtained for BRNN model. Hence based on R^2, MAE and MAPE of testing data set, it is found that the BRNN model is more efficient than any other model considered, in predicting the non-dimensional transient settlement followed by LMNN, MGGP, SVR and MARS.

6. Sensitivity analysis

Sensitivity analysis is performed to observe the influence of each input on the output parameter (((*sf*/*su*) %)) and also to determine the most influencing parameter. Pearson's correlation coefficients as mentioned in Fig. 10

Parameters	FS	D_f/B	$q_{d(max)}/q_u$ (%)	D_r (%)	s_f/s_u (%)
FS	1				
D_f/B	0	1			
$q_{d(max)}/q_u$ (%)	0	0	1		
D_r (%)	0	0	0	1	
s_f/s_u (%)	-0.907	-0.072	0.277	-0.065	1

Fig. 10 Correlation matrix of the present data

Table 7 Relative importance based on Garson's algorithm and connection weight approach

Method	Parameters	Garson's algorithm	Connection weight
LMNN	FS	34.108	-1.777
	D_f/B	29.803	-1.096
	$q_{d(max)}/q_u$ (%)	8.560	0.425
	D_r(%)	27.529	-0.099
BRNN	FS	33.863	-1.431
	D_f/B	19.017	-0.044
	$q_{d(max)}/q_u$ (%)	8.859	0.315
	D_r(%)	38.261	0.218

Table 8 Parameter importance based on the MARS model

Parameters	nsubsets	GCV	RSS
FS	7	100.0	100.0
$q_{d(max)}/q_u$ (%)	5	34.6	34.1
D_r(%)	3	14.9	15.3
D_f/B	2	8.8	9.9

indicate the correlations among the inputs and the output. Based on the weights and biases obtained from the neural networks (LMNN, BRNN), the relative importance of inputs is listed in Table 7 using two well-known procedures viz. Garson's algorithm as well as Connection weight approach. Both the methods have been carried out following procedures mentioned in Olden *et al.* (2004). Pearson's correlation coefficient indicate that FS is the most significant parameter influencing (s_f/s_u)% followed by $q_{d(max)}/q_u$ (%), D_f/B and D_r (%). From Table 7, it is interpreted that for both LMNN and BRNN methods, FS is the most significant input parameter. The connection weight approach also suggests FS as the most important

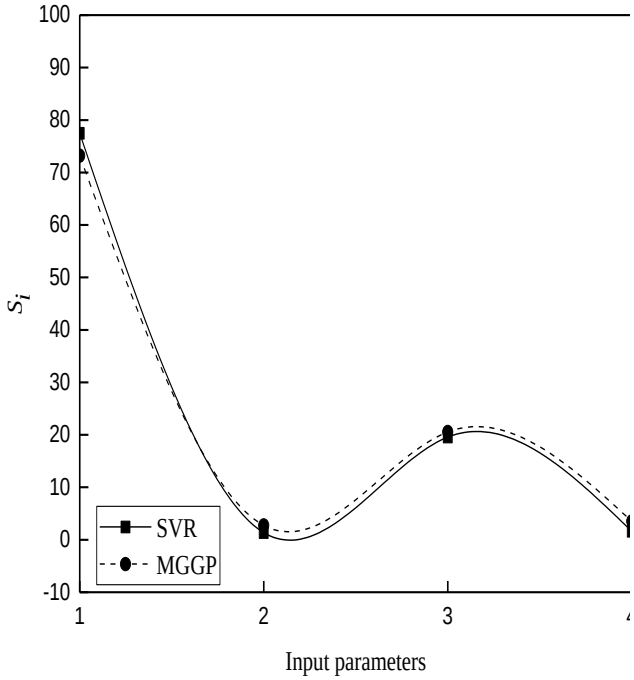

Fig. 11 Sensitivity of Input parameters (SVR and MGGP)

parameter. Therefore, based on values of Fig. 10 and Table 7, it can be inferred that the transient settlement of footing is primarily controlled by the static load on that foundation.

For MARS, the variable importance is obtained using "evimp" function in R. This function determines the variable importance in terms of nsubsets, GCV and Residual sum squared (RSS). The nsubsets is the number of subsets chosen after the pruning pass. The values of the three parameters, obtained using the "evimp" function are tabulated in Table 8. It is observed that the most important parameter is FS followed by $q_{d(max)}/q_u$ (%), D_r (%) and D_f/B.

The sensitivities of input parameters based on SVR and MGGP model are calculated using Eq. (20). Eq. (20) was given by Beura and Bhuyan (2018) using the concepts of Gandomi *et al.* (2013). Positive value of D_i indicates positive influence of i^{th} variable and negative value of D_i indicate reverse influence.

$$S_i = \frac{|D_i|}{\sum_{i=1}^{n}|D_i|} \times 100 \tag{20}$$

where $D_i = f_{max}(\upsilon_i) - f_{min}(\upsilon_i)$

υ_i = input variable (i =1, 2…. n)

$f_{max}(\upsilon_i)$ = model output (for maximum value of i^{th} input variable and mean values of remaining input variable)

$f_{min}(\upsilon_i)$ = model output (for minimum value of i^{th} input variable and mean values of remaining input variable)

Fig. 11 represents variation of S_i for different input parameters for both SVR model and MGGP model. In abscissa of Fig. 11, input parameters 1, 2, 3 and 4 correspond to factor of safety (FS), embedment ratio (D_f/B), intensity of cyclic load ($q_{d(max)}/q_u$ (%)) and relative

density (D_r (%)) respectively. It is observed that the output is most sensitive to *FS* followed by $q_{d(max)}/q_u$ (%), D_r (%) and D_f/B. For MGGP model D_i values for *FS*, D_f/B, $q_{d(max)}/q_u$ (%) and D_r (%) are found to be -7.981, -0.299, 2.238, -0.383 respectively. Similarly, for SVR mode D_i values for *FS*, D_f/B, $q_{d(max)}/q_u$ (%) and D_r (%) are found to be -6.898, -0.120, 1.743 and -0.143 respectively. Hence, sensitivity analysis of both MGGP and SVR model indicates that only $q_{d(max)}/q_u$ (%) has positive influence on the output whereas *FS*, D_f/B, and D_r (%) inversely influence the output.

7. Conclusions

A data set generated using Finite Element Model is analyzed with the help of five artificial intelligence (AI) techniques. A comparison is established among the models to find out the best algorithm for soil dynamics problems like transient response of shallow foundation. Model equations have been formulated to calculate the non-dimensional transient settlement ((s_f/s_u) %) of strip footing. Sensitivity analysis (SA) is carried out to pick the most influencing parameter. Based on the outcomes from different AI techniques and sensitivity analysis following major inferences are drawn;

• Transient settlement response of shallow foundation can successfully be predicted with reasonable accuracy using neural networks, SVM, MARS and MGGP.

• Based on the R^2, MAE and MAPE of testing data sets, the BRNN method is found to be the best method to estimate non-dimensional transient settlement ((s_f/s_u) %) of strip foundation.

• Pearson's correlation coefficients indicate that *FS* is the most important input parameter influencing the non-dimensional settlement ((s_f/s_u) %), followed by intensity of cyclic load ($q_{d(max)}/q_u$ (%)), embedment ratio (D_f/B) and relative density (D_r (%)).

• Sensitivity analysis on SVR, MARS and MGGP models indicates that the transient settlement is highly influenced by the amount of allowable static load applied on the foundation, followed by intensity of cyclic load ($q_{d(max)}/q_u$ (%)), relative density (D_r (%)) and embedment ratio (D_f/B).

• Based on the D_i values obtained from the MGGP and SVR model it can be concluded that, among all the parameters considered, intensity of cyclic load ($q_{d(max)}/q_u$ (%)) is the only parameter that positively influences the non-dimensional transient settlement (s_f/s_u (%)).

The study will be helpful in preliminary estimation of transient settlement under vertical cyclic load in order to flourish laboratory model tests as well as proper selection of parameters. The calculation of transient settlement will not only be helpful in deciding the life time of foundation but also will guide a practicing engineer to consider possible replacement of subsoil. In addition, knowledge of important parameters will expedite the overall design of foundation. The use of different AI techniques for the settlement analysis of the foundations supporting structures in seismic prone areas can be an interesting research area in future.

References

Alavi, A.H., Hasni, H., Zaabar, I. and Lajnef, N. (2017), "A new approach for modeling of flow number of asphalt mixtures", *Arch. Civil Mech. Eng*., **17**(2), 326-335. https://doi.org/10.1016/j.acme.2016.06.004.

Allotey, N. and El Naggar, M.H. (2008), "An investigation into the Winkler modeling of the cyclic response of rigid footings", *Soil Dyn. Earthq. Eng.,* **28**(1), 44-57. https://doi.org/10.1016/j.soildyn.2007.04.003.

Behera, R.N. and Patra, C.R. (2018), "Ultimate bearing capacity prediction of eccentrically inclined loaded strip footings", *Geotech. Geol. Eng*., **36**(5), 3029-3080. https://doi.org/10.1007/s10706-018-0521-z.

Beura, S.K. and Bhuyan, P.K. (2018), "Operational analysis of signalized street segments using multi-gene genetic programming and functional network techniques", *Arab. J. Sci. Eng*., **43**(10), 5365-5386. https://doi.org/10.1007/s13369-018-3176-4.

Bui, D.K., Nguyen, T., Chou, J.S., Nguyen-Xuan, H. and Ngo, T.D. (2018), "A modified firefly algorithm-artificial neural network expert system for predicting compressive and tensile strength of high-performance concrete", *Constr. Build. Mater*., **180**, 320-333. https://doi.org/10.1016/j.conbuildmat.2018.05.201.

Das, B.M. (2016), *Principle of Foundation Engineering*, Eighth Edition, Cengage Learning.

Das, B.M., Yen, S.C. and Singh, G. (1995), "Settlement of shallow foundation on sand due to cyclic loading", *Proceedings of the International Conference on Recent Advances in Geotechnical Earthquake Engineering and Soil Dynamics*.

Das, S.K. and Basudhar, P.K. (2008), "Undrained lateral load capacity of piles in clay using artificial neural network", *Comput. Geotech*., **33**(8), 454-459. https://doi.org/10.1016/j.compgeo.2006.08.006.

Das, S.K. and Sabat, A.K. (2008), "Using neural networks for prediction of some properties of fly ash", *Elect. J. Geotech. Eng*., **13**, 1-14.

Das, S.K., Samui, P. and Sabat, A.K. (2011) "Application of artificial intelligence to maximum dry density and unconfined compressive strength of cement stabilized soil", *Geotech. Geol. Eng*., **29**(3), 329-342. https://doi.org/10.1007/s10706-010-9379-4.

Das, S.K., Samui, P. and Sabat, A.K. (2011), "Prediction of field hydraulic conductivity of clay liners using an artificial neural network and support vector machine", *Int. J. Geomech*., **12**(5), 606-611. https://doi.org/10.1061/(ASCE)GM.1943-5622.0000129.

Das, S.K., Samui, P., Sabat, A.K. and Sitharam, T.G. (2010) "Prediction of swelling pressure of soil using artificial intelligence techniques", *Environ. Earth Sci*., **61**(2), 393-403. https://doi.org/10.1007/s12665-009-0352-6.

Dimitriadou, E., Hornik, K, Leisch, F, Meyer, D, Weingessel, A. and Leisch, M.F. (2009), Package "e1071". R Software Package. http://cran.rproject.org/web/packages/e1071/index.Html.

EPRI (1990), *Manual on Estimating Soil Properties for Foundation Desig*n. Electric Power Research Institute, Palo Alto, California, U.S.A.

Erzin, Y, and Gul, T. (2013), "The use of neural networks for the prediction of the settlement of pad footings on cohesionless soils based on standard penetration test", *Geomech. Eng*., **5**(6), 541-564. http://doi.org/10.12989/gae.2013.5.6.541.

Erzin, Y. and Gul, T.O. (2014), "The use of neural networks for the prediction of the settlement of one-way footings on cohesionless soils based on standard penetration test", *Neural Comput. Appl.*, **24**(3-4), 891-900. https://doi.org/10.1007/s00521-012-1302-x.

Friedman, J. H. (1991) "Multivariate adaptive regression splines", *Annals Stat.*, **19**(1), 1-67.

Gandomi, A.H. and Alavi, A.H. (2012a), "A new multi-gene genetic programming approach to nonlinear system modeling Part I, materials and structural engineering problems", *Neural Comput. Appl.*, **21**(1), 171-187. https://doi.org/10.1007/s00521-011-0734-z.

Gandomi, A.H. and Alavi, A.H. (2012b), "A new multi-gene genetic programming approach to non-linear system modeling. Part II, geotechnical and earthquake engineering problems", *Neural Comput. Appl.*, **21**(1), 189-201. https://doi.org/10.1007/s00521-011-0735-y.

Gandomi, A.H., Yun, G.J. and Alavi, A. H. (2013), "An evolutionary approach for modeling of shear strength of RC deep beams", *Mater. Struct.,* **46**(12), 2109-2119. https://doi.org/10.1617/s11527-013-0039-z.

Gao, W. and Chen, D. (2019), "Prediction model of service life for tunnel structures in carbonation environments by genetic programming", *Geomech. Eng.*, **18**(4), 373-389. https://doi.org/10.12989/gae.2019.18.4.373.

Garg, A., Garg, A, Tai, K. and Sreedeep, S. (2014b), "Estimation of pore water pressure of soil using genetic programming", *Geotech. Geol. Eng.*, **32**(4), 765-772. https://doi.org/10.1007/s10706-014-9755-6.

Garg, A., Garg, A, Tai, K., Barontini, S. and Stokes, A. (2014a), "A computational intelligence-based genetic programming approach for the simulation of soil water retention curves", *Transport Porous Media*, **103**(3), 497-513. https://doi.org/10.1007/s11242-014-0313-8.

Gazetas, G. (1991) "Formulas and charts for impedances of surface and embedded foundations", *J. Geotech. Eng.*, **117**(9), 1363-1381. https://doi.org/10.1061/(ASCE)0733-9410(1991)117:9(1363).

Ghanizadeh, A.R., Abbaslou, H., Amlashi, A.T. and Alidoust, P. (2019), "Modeling of bentonite/sepiolite plastic concrete compressive strength using artificial neural network and support vector machine." *Front. Struct. Civ. Eng.,* **13**(1), 215-39. https://doi.org/10.1007/s11709-018-0489-z.

Goh, A.T., Kulhawy, F.H. and Chua, C.G. (2005), "Bayesian neural network analysis of undrained side resistance of drilled shafts", *J. Geotech. Geoenviron. Eng.*, **131**(1), 84-93. https://doi.org/10.1061/(ASCE)1090-0241(2005)131:1(84).

Golafshani, E.M. and Behnood, A. (2018), "Application of soft computing methods for predicting the elastic modulus of recycled aggregate concrete", *J. Cleaner Prod.*, **176**, 1163-1176. https://doi.org/10.1016/j.jclepro.2017.11.186.

Harden, C., Hutchinson, T., Martin, G. R. and Kutter, B. L. (2005), "Numerical modeling of the nonlinear cyclic response of shallow foundations", Report No 2005/04 Pacific Earthquake Engineering Research Center (PEER) Berkeley California, U.S.A.

Hasanipanah, M., Keshtegar, B., Thai, D.K. and Troung, N.T. (2020), "An ANN-adaptive dynamical harmony search algorithm to approximate the flyrock resulting from blasting", *Eng. Comput.*, 1-13. https://doi.org/10.1007/s00366-020-01105-9.

Kaveh, A., Hamze-Ziabari, S.M. and Bakhshpoori, T. (2018), "Soft computing-based slope stability assessment: A comparative study", *Geomech. Eng.*, **14**(3), 257-269. http://doi.org/10.12989/gae.2018.14.3.257.

Khademi, F., Akbari, M., Jamal, S.M. and Nikoo, M. (2017), "Multiple linear regression, artificial neural network, and fuzzy logic prediction of 28 days compressive strength of concrete", *Front. Struct. Civ. Eng.*, **11**(1), 90-99. https://doi.org/10.1007/s11709-016-0363-9.

Khorrami, R. and Derakhshani, A. (2019), "Estimation of ultimate bearing capacity of shallow foundations resting on cohesionless soils using a new hybrid M5'-GP model", *Geomech. Eng.*, **19**(2), 127-139. https://doi.org/10.12989/gae.2019.19.2.127.

Kurnaz, T. F. and Kaya, Y. (2018), "The comparison of the performance of ELM, BRNN, and SVM methods for the prediction of compression index of clays", *Arab. J. Geosci.*, **11**(24), 770. https://doi.org/10.1007/s12517-018-4143-9.

Luat, N.V., Lee, J., Lee, D.H. and Lee, K. (2020d), "GS-MARS method for predicting the ultimate load-carrying capacity of rectangular CFST columns under eccentric loading", *Comput. Concrete*, **25**(1), 1-14. doi: https://doi.org/10.12989/cac.2020.25.1.001.

Luat, N.V., Lee, K. and Thai, D.K. (2020a), "Application of artificial neural networks in settlement prediction of shallow foundations on sandy soils", *Geomech. Eng.*, **20**(5), 385-397. https://doi.org/10.12989/gae.2020.20.5.385.

Luat, N.V., Nguyen, V.Q., Lee, S., Woo, S. and Lee, K. (2020c), "An evolutionary hybrid optimization of MARS model in predicting settlement of shallow foundations on sandy soils", *Geomech. Eng.*, **21**(6), 583-598. https://doi.org/10.12989/gae.2020.21.6.583.

Luat, N.V., Shin, J. and Lee, K. (2020b), "Hybrid BART-based models optimized by nature-inspired metaheuristics to predict ultimate axial capacity of CCFST columns", *Eng. Comput.*, **1**-30. https://doi.org/10.1007/s00366-020-01115-7.

Meyerhof, G.G. (1963), "Some recent research on the bearing capacity of foundations", *Can. Geotech. J.*, **1**(1), 16-26. https://doi.org/10.1139/t63-003.

Milborrow, S. (2019), Package "earth", R Software Package.

Muduli, P.K. and Das, S.K. (2015), "Model uncertainty of SPT-based method for evaluation of seismic soil liquefaction potential using multi-gene genetic programming", *Soils Found.*, **55**(2), 258-275. https://doi.org/10.1016/j.sandf.2015.02.003.

Muduli, P.K., Das, M.R., Das, S.K. and Senapati, S. (2015), "Lateral load capacity of piles in clay using genetic programming and multivariate adaptive regression spline", *Ind. Geotech. J.*, **45**(3), 349-359. https://doi.org/10.1007/s40098-014-0142-2.

Naderpour, H., Poursaeidi, O. and Ahmadi, M. (2018), "Shear resistance prediction of concrete beams reinforced by FRP bars using artificial neural networks", *Measurement*, **126**, 299-308. https://doi.org/10.1016/j.measurement.2018.05.051.

Naderpour, H., Rafiean, A.H. and Fakharian, P. (2018), "Compressive strength prediction of environmentally friendly concrete using artificial neural networks", *J. Build. Eng.*, **16**, 213-219. https://doi.org/10.1016/j.jobe.2018.01.007.

Nguyen, K.T., Nguyen, Q.D., Le, T.A., Shin, J. and Lee, K. (2020), "Analyzing the compressive strength of green fly ash based geopolymer concrete using experiment and machine learning approaches", *Constr. Build. Mater.*, **247**, 118581. https://doi.org/10.1016/j.conbuildmat.2020.118581.

Nguyen, M.S.T., Thai, D.K. and Kim, S.E. (2020), "Predicting the axial compressive capacity of circular concrete filled steel tube columns using an artificial neural network", *Steel Compos. Struct.*, **35**(3), 415-437. https://doi.org/10.12989/scs.2020.35.3.415.

Olden, J.D., Joy, M.K. and Death, R.G. (2004), "An accurate comparison of methods for quantifying variable importance in

artificial neural networks using simulated data", *Ecol. Modell.*, **178**(3-4), 389-397. https://doi.org/10.1016/j.ecolmodel.2004.03.013.

Omar, M., Hamad, K., Al Suwaidi, M. and Shanableh, A. (2018), "Developing artificial neural network models to predict allowable bearing capacity and elastic settlement of shallow foundation in Sharjah, United Arab Emirates", *Arab. J. Geosci.*, **11**(16), 464. https://doi.org/10.1007/s12517-018-3828-4.

OpenSees [Computer Program]. Open System for Earthquake Engineering Simulation, Pacific Earthquake Engineering Research Center (PEER), University of California, Berkeley, U.S.A. http,//OpenSees.berkeley.edu.

Patra, C., Behera, R., Sivakugan, N. and Das, B. (2012), "Ultimate bearing capacity of shallow strip foundation under eccentrically inclined load, Part I", *Int. J. Geotech. Eng.*, **6**(3), 343-352. https://doi.org/10.3328/IJGE.2012.06.03.343-352 .

Rabiei, M. and Choobbasti, A.J. (2020), "Innovative piled raft foundations design using artificial neural network", *Front. Struct. Civ. Eng.*, **14**(1), 138-146. https://doi.org/10.1007/s11709-019-0585-8.

Raychowdhury, P. (2008), "Nonlinear Winkler-based shallow foundation model for performance assessment of seismically loaded structures", Ph. D Dissertation. University of California, San Diego, San Diego, California, U.S.A.

Raymond, G.P. and Komos, F.E. (1978), "Repeated load testing of a model plane strain footing", *Can. Geotech. J.*, **15**(2), 190-201. https://doi.org/10.1139/t78-019.

Sahu, R., Patra, C.R., Das, B.M. and Sivakugan, N. (2016), "Bearing capacity of shallow strip foundation on geogrid-reinforced sand subjected to inclined load", *Int. J. Geotech. Eng.*, **10**(2), 183-189. https://doi.org/10.1080/19386362.2015.1105622.

Samadi, M., Jabbari, E., Azamathulla, H.M. and Mojallal, M. (2015), "Estimation of scour depth below free overfall spillways using multivariate adaptive regression splines and artificial neural networks", *Eng. Appl. Comput. Fluid Mech.* **9**(1), 291-300. https://doi.org/10.1080/19942060.2015.1011826.

Samui, P. (2008), "Support vector machine applied to settlement of shallow foundations on cohesionless soils", *Comput. Geotech.*, **35**(3), 419-427. https://doi.org/10.1016/j.compgeo.2007.06.014.

Samui, P., Sitharam, T.G. and Kurup, P.U. (2008), "OCR prediction using support vector machine based on piezocone data", *J. Geotech. Geoenviron. Eng.*, **134**(6), 894-898. https://doi.org/10.1061/(ASCE)1090-0241(2008)134:6(894).

Sasmal, S.K. and Behera, R.N. (2018), "Prediction of combined static and cyclic load-induced settlement of shallow strip footing on granular soil using artificial neural network", *Int. J. Geotech. Eng.* https,//doi.org/10.1080/19386362.2018.1557384.

Searson, D.P. (2009), *GPTIPS, Genetic Programming and Symbolic Regression for MATLAB*.

Searson, D.P., Leahy, D.E. and Willis, M.J. (2010), "GPTIPS an open source genetic programming toolbox for multigene symbolic regression", *Proceedings of the International Multi Conference of Engineers and Computer Scientists*, Hong Kong, China, March.

Shahin, M.A. (2015), "A review of artificial intelligence applications in shallow foundations", *Int. J. Geotech. Eng.*, **9**(1), 49-60. https://doi.org/10.1179/1939787914Y.0000000058.

Shahin, M.A., Jaksa, M.B. and Maier, H.R. (2002), "Artificial neural network based settlement prediction formula for shallow foundations on granular soils", *Australian Geomech. J. News Australian Geomech. Soc.*, **37**(4), 45-52.

Smola, A.J. and Schölkopf, B. (2014), "A tutorial on support vector regression", *Statist. Comput.*, **14**(3), 199-222. https://doi.org/10.1023/B:STCO.0000035301.49549.88.

Tran, V. L., Thai, D.K. and Kim, S.E. (2019b) "A new empirical formula for prediction of the axial compression capacity of CCFT columns", *Steel Compos. Struct.*, **33**(2), 181-194. https://doi.org/10.12989/scs.2019.33.2.181.

Tran, V. L., Thai, D.K. and Nguyen, D.D. (2020), "Practical artificial neural network tool for predicting the axial compression capacity of circular concrete-filled steel tube columns with ultra-high-strength concrete", *Thin-Walled Struct.*, **151**, 106720. https://doi.org/10.1016/j.tws.2020.106720.

Tran, V.L., Thai, D.K. and Kim, S.E. (2019a), "Application of ANN in predicting ACC of SCFST column", *Compos. Struct.*, **228**, 111332. https://doi.org/10.1016/j.compstruct.2019.111332.

Vapnik, V., Golowich, S.E. and Smola, A.J. (1997), *Support Vector Method for Function Approximation, Regression Estimation and Signal Processing*, in *Advances in Neural Information Processing Systems,* 281-287.

Won, J. and Shin, J. (2021), "Machine Learning-Based Approach for Seismic Damage Prediction Method of Building Structures Considering Soil-Structure Interaction", *Sustainability*, **13**(8), 4334. https://doi.org/10.3390/su13084334.

Xu, J., Ren, Q. and Shen, Z. (2017), "Sensitivity analysis of the influencing factors of slope stability based on LS-SVM", *Geomech. Eng.*, **13**(3), 447-458. https://doi.org/10.12989/gae.2017.13.3.447.

Zhang, C., Ji, J., Gui, Y., Kodikara, J., Yang, S. Q. and He, L. (2016), "Evaluation of soil-concrete interface shear strength based on LS-SVM", *Geomech. Eng.*, **11**(3), 361-372. http://doi.org/10.12989/gae.2016.11.3.361.

Zhang, W. and Goh, A.T. (2016), "Multivariate adaptive regression splines and neural network models for prediction of pile drivability", *Geosci. Front.*, **7**(1), 45-52. https://doi.org/10.1016/j.gsf.2014.10.003.

CC

Appendix

Table A Dataset used for training and testing

Data type	FS	D_f/B	q_{dmax}/q_u (%)	D_r (%)	s_f/s_u(%)
	2	1	10	69	9.565
	3.5	0	5	35	2.562
	3.5	0.5	5	51	1.824
	2	0.5	13	69	12.325
	2.5	1	10	69	5.899
	2.5	1	10	35	6.581
	2.5	1	13	35	7.633
	3.5	1	10	35	2.594
	3	0	13	35	5.625
	2.5	1	13	69	6.710
	2.5	0.5	10	35	6.882
	3	0.5	5	35	3.023
	2.5	0	5	69	5.242
	3	0	5	51	3.175
	3.5	1	10	51	2.702
	2.5	0.5	13	51	6.093
	3	1	10	35	4.149
	2	1	13	51	11.988
	2	0	5	51	9.200
	3.5	1	10	69	2.562
	2	1	5	69	7.975
	2	0	13	51	12.442
	3.5	0.5	5	35	2.345
	3	0	5	35	3.384
	2	0	5	35	10.240
	2	0	5	69	8.966
	2	0.5	5	51	7.229
	3.5	0	10	69	2.839
Training	2	1	10	35	10.971
	2.5	0	10	35	7.474
	2.5	0.5	10	51	5.318
	2.5	0	13	35	8.638
	3	0	13	51	5.137
	3	0	5	69	3.217
	2	0	10	51	11.122
	3	0	10	35	4.668
	3	0.5	13	51	4.058
	2.5	0.5	10	69	6.593
	2	0.5	13	35	12.878
	3.5	1	13	35	3.343
	2	0.5	10	69	10.757
	2.5	0	10	51	6.755
	3	0	10	51	4.312
	2	0	13	35	14.025
	3.5	1	5	51	2.268
	2	0	10	35	12.486
	2.5	0	5	51	5.289
	3.5	1	5	35	2.238
	3.5	0	13	35	3.761
	2.5	1	5	69	4.694
	3.5	0.5	10	51	2.206
	3.5	0	10	35	2.943
	2	0.5	5	69	8.926
	2	1	13	35	12.318
	3	0.5	5	69	3.176
	3.5	0.5	10	35	2.713
	2.5	1	5	51	5.135

	3	0	10	69	4.287
	3	1	10	69	3.849
	2	0.5	5	35	9.416
	2.5	1	13	51	7.467
	3.5	0	13	69	3.480
	2	1	5	51	8.892
	3.5	0	10	51	2.760
	2.5	0	10	69	6.616
	2.5	0	13	51	7.726
	3.5	0.5	13	35	3.483
	3.5	0.5	13	51	2.766
	2	0.5	10	35	11.488
	3	1	13	51	4.981
	3	0.5	5	51	2.452
	3	1	10	51	4.191
	2	0.5	10	51	8.739
	2.5	0.5	13	35	7.939
	2.5	1	10	51	6.538
	3	0.5	13	69	5.050
	2.5	0	13	69	7.542
	2.5	1	5	35	5.099
	3	0.5	10	51	3.415
	2.5	0.5	13	69	7.507
	3	1	5	69	2.882
	3.5	0	5	69	2.355
	3.5	0.5	5	69	2.360
	3	0.5	10	35	4.330
	2.5	0.5	5	69	5.234
	3	1	13	69	4.528
	3	0	13	69	5.061
	3.5	1	13	69	3.133
	2	1	5	35	8.998
	3	1	5	51	3.029
	3	1	5	35	2.886
	3.5	1	5	69	2.119
	3.5	1	13	51	3.391
	3.5	0.5	13	69	3.481
Testing	2.5	0.5	5	35	5.324
	2	1	10	51	10.721
	3	0.5	13	35	5.206
	3	0.5	10	69	4.285
	3.5	0.5	10	69	2.828
	2	0	13	69	12.086
	2.5	0.5	5	51	4.175
	2	0	10	69	10.758
	3.5	0	5	51	2.329
	3.5	0	13	51	3.486
	3	1	13	35	4.983
	2	1	13	69	10.660
	2.5	0	5	35	5.772
	2	0.5	13	51	9.768